Physica B 456 (2015) 293–297

Contents lists available at ScienceDirect

Physica B

journal homepage: www.elsevier.com/locate/physb

Structure and magnetic properties of highly textured nanocrystalline Mn–Zn ferrite thin film

Jaison Joseph [a,*], R.B. Tangsali [b], V.P. Mahadevan Pillai [c], R.J. Choudhary [d], D.M. Phase [d], V. Ganeshan [d]

[a] Department of Physics, Goverment College, Khandola, Goa 403107 India
[b] Department of Physics, Goa University, Taleigao Plateau, Goa 403206 India
[c] Department of Optoelectronics, University of Kerala,Thiruvananthapuram, Kerala 695581 India
[d] UGC-DAE-CSR Indore, Madhya Pradesh 452017 India.

ARTICLE INFO

Article history:
Received 23 June 2014
Received in revised form
8 September 2014
Accepted 10 September 2014
Available online 19 September 2014

Keywords:
Nanocrystalline
Thin films
Texture
Magnetic properties

ABSTRACT

Nanoparticles of $Mn_{0.2}Zn_{0.8}Fe_2O_4$ were chemically synthesized by co-precipitating the metal ions in aqueous solutions in a suitable alkaline medium. The identified XRD peaks confirm single phase spinal formation. The nanoparticle size authentication is carried out from XRD data using Debye Scherrer equation. Thin film fabricated from this nanomaterial by pulse laser deposition technique on quartz substrate was characterized using XRD and Raman spectroscopic techniques. XRD results revealed the formation of high degree of texture in the film. AFM analysis confirms nanogranular morphology and preferred directional growth. A high deposition pressure and the use of a laser plume confined to a small area for transportation of the target species created certain level of porosity in the deposited thin film. Magnetic property measurement of this highly textured nanocrystalline Mn–Zn ferrite thin film revealed enhancement in properties, which are explained on the basis of texture and surface features originated from film growth mechanism.

1. Introduction

The growth of soft magnetic ferrite thin films on amorphous substrates find scientific interest due to its potential commercial applications in magnetic thin film read heads, micro-inductors and micro-transformers [1–6]. This interest also stems from the fact that the magnetic properties in thin films show discrepancies such as lower saturation magnetization and higher coercivity in comparison to its corresponding bulk materials. Ferrite films also find applications in microwave acoustic and short wavelength magnetostatic wave devices, wherein the current bulk ferrite components are not compatible with planar circuit design [7]. Relatively high resistivity and permeability of spinel ferrites in thin film form make it a preferred material for soft magnetic under layers in perpendicular magnetic recording media [8].

Many industrial applications require ferrite thin films to be grown with processes compatible with integrated circuit technology on amorphous substrates. To avoid unwanted chemical reactions with the metal atoms involved in device structures during the integration of magnetic oxides with semiconducting materials, low processing temperature is a preferred prerequisite. An increased mobility for the deposited atoms on the film surface results in creation of homogeneous film microstructure, maintaining the stoichiometry of the target. The high kinetic energy of the vaporized materials in laser plume, offers pulse laser deposition (PLD) the processing advantages favorable for above requirements. It has been further suggested that this technique may possibly lower the substrate processing temperature required for crystallization [9]

Manganese zinc ferrite (Mn–Zn ferrite) is one prominent soft magnetic material known for its high permeability, large resistivity, relatively high magnetization and low coercivity. It finds applications in magnetic sensors, reading heads for magnetic recording media, switch mode power supplies, deflection yoke rings and spintronic devices [10,11–14]. High quality Mn–Zn ferrite thin films find process applications for the miniaturization of complex geometrical devices. For example, in the arena of magnetic recording, a possible thermally assisted magnetic recording method can overcome the thermal agitation limit of recording media to achieve a higher recording density beyond Tb/inch^2 by applying the magnetic recording field and the laser beam to the same position on the recording media [15]. Incorporating a

* Corresponding author. Tel./fax: +91 8322287718.
E-mail address: jaisonjosephp@gmail.com (J. Joseph).

http://dx.doi.org/10.1016/j.physb.2014.09.015
0921-4526/

magnetic core in the recording head for a sufficiently large recording field, could possibly interfere with the optical path of the laser beam. Mn–Zn ferrite thin film which is a transparent magnetic material with a high M_s and high resistivity could possibly be a potential candidate for use as a magnetic core that will not interrupt the laser beam [16].

Based on thin film preparation conditions such as substrate temperature, pressure, growth rate, shadowing effects etc. and depending on the film growth methods one can obtain significantly different surface morphologies and film microstructures [17]. In an event of non-commencement of epitaxial growth of a film in the layer-by-layer mode, the growth front can be rough in the form of mounds. Further a noise induced roughening during the growth can lead to the formation of self-affine fractal morphologies [18]. Another factor that strongly alters the growth characteristics is the kinetic effect stress relaxation in between film interfaces. These inherently related dynamic growth mechanisms have a significant and generally different influence on the physical properties of the material in thin film format [19].

Since magnetic properties play an important role in industrial applications related to magnetic recordings and magnetic memories, the amount of disorder at the surface influencing magnetic properties in thin films attain reasonable significance. The size, shape and grain orientation define the microstructure dependent property of any single phase polycrystalline material. In films with reduced grain sizes such as nanocrystalline ferrite thin films the role of grain boundaries is expected to gain significant importance. In comparison to a bulk material the grain boundaries occupy a significant volume in thin films. Therefore it is expected to observe a reasonable change in property due to altered grain boundary structures in thin films even though the grain size, chemical composition and phase remain the same. Hence we viewed the deposition of nanocrystalline ferrite thin film with a manifestation of high crystallographic texture as an interesting feature for investigation and studied its magnetic properties. In the present paper we report an enhanced coercivity.

2. Experimental

Nanoparticle $Mn_{0.2}Zn_{0.8}Fe_2O_4$ ferrite material was prepared in our laboratory by co-precipitating aqueous solutions of $ZnSO_4$, $MnCl_2$ and $FeCl_3$ mixtures in alkaline medium. The powdered sample of prepared material was characterized using Rigaku X-ray diffractometer (XRD) with a high intensity rotating anode X-ray source. The powdered sample was palletized at 15 T pressure and sintered at 450 °C temperature which was used as a target material for laser ablation. The laser ablation was carried out using Excimer laser KrF (248 nm) (Lambda Physik COMPex 201 model) in a chamber maintaining the pressure at 2×10^{-6} T on a quartz substrate elevated to a temperature of 450 °C. The deposition was performed for 30 min keeping the substrate at a distance of 4.5 cm from target and retaining laser energy at 220 mJ with a repeation rate of 10 Hz. The focused laser beam was incident on the target surface at an angle of 45°. The target was rotated at 10 rpm with the substrate mounted opposite to the target on a heater plate using silver paint. After deposition, the thin film was cooled down to room temperature at a rate of 5 °C/min, maintaining vacuum in deposition chamber. The prepared thin film was characterized using standard $\theta/2\theta$ XRD using Bruker AXE D8 X-ray Diffractometer with Cu Kα radiation at room temperature. Raman spectroscopic measurements of thin film was obtained on HORIBA Jobin Yvon LabRAM HR 800 Micro Raman spectrometer with Argon Iron Laser source having wavelength 514 nm in a spectral resolution of 1 cm^{-1}. The thickness measurement of the film was carried out on an AMBIOS XP-1 stylus profiler with 0.5 nm resolution. The AFM image of the film taken on SPM (Digital Nano-Scope-III) in contact mode was used for film surface analysis and particle size determination. Magnetic measurements were carried out on Quantum Design's MPMS SQUID VSM.

3. Results and discussion

The X-ray diffraction pattern of $Mn_{0.2}Zn_{0.8}Fe_2O_4$ target material in powder form along with that of deposited thin film on quartz substrate is shown in Fig. 1.

The positions of the observed peaks are in agreement with the peaks reported in JCPDS files which confirm the single phase cubic spinel structure of the target sample. The interplanar spacing (d) is calculated in accordance with Bragg's law and hence the average lattice parameter (a) is obtained using the equation given below:

$$\frac{1}{d_{hkl}}=\frac{\sqrt{h^2+k^2+l^2}}{a} \quad (1)$$

The particle sizes of the sample was determined by the Debye Scherrer formula given below by averaging the overall seven major spinnel peaks.

$$D=\frac{0.9\lambda}{\beta\ \mathrm{Cos}\ \theta} \quad (2)$$

The lattice constant and particle size is tabulated in Table 1.

From the observation of a single XRD peak (311), the crystal structure of the thin film appears to be highly textured. In PLD process, strain may be induced during the film growth, wherein the ablation temperature is lower than the melting temperature of the target material. In such cases the film growth is far from equilibrium and the ablated material particles do not have enough mobility to achieve the lowest thermal dynamic energy state. During the deposition of the thin film a large strain could be induced in the interface between the film and the quartz substrate at the initial stage of growth. Further, the difference of thermal coefficient between the film and quartz substrate may also induce strain/stress during film growth. Since the film was deposited at optimized temperature and deposition rate, the formation of 311 texture is attributed to the minimization of strain energy density [20].

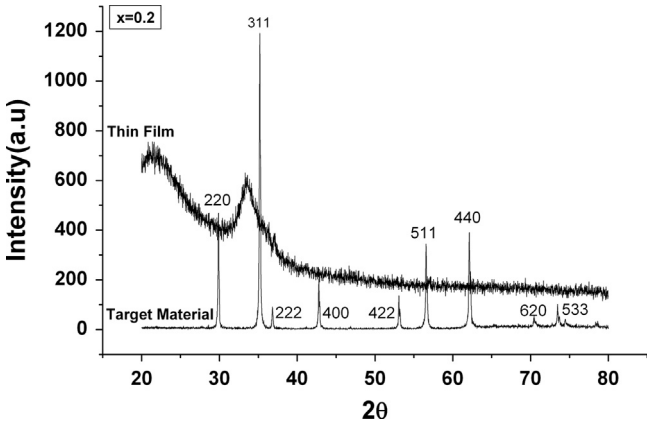

Fig. 1. XRD pattern of $Mn_{0.2}Zn_{0.8}Fe_2O_4$.

Table 1
Lattice constant and particle size of target material.

Lattice constant, *a* (Å)	Particle size, *D* nm
8.474829	44.00

It is observed that there is an appreciable shift in peak position (blue shift) for thin film 311 peak in comparison to the target material. This peak shift arising out of swing towards large inter-reticular distance can be explained with the help of atomic peening phenomena [21]. The deposition of the target species on substrate using PLD involves disintegration of the species from the target by high energy pulsed laser, transportation of the same through the laser plume and its deposition onto the substrate preceded by a bombardment. A bombardment on the substrate layer by energetic species generates a compressive stress in crystal planes parallel to the film surface, which in turn generates an expansion in the planes normal to the surface. This results in an increase of the lattice parameter normal to the surface, which explains the shift observed in thin film [22,23]. Pictographic representation of the suggested phenomenon in Fig. 2 provides a visual representation of the happening wherein a_0, represent lattice parameter of the unstressed structure, $a_\perp$ lattice parameter normal to the surface, and $a_{//}$ lattice parameter parallel to the surface.

Thickness of the prepared thin film determined on stylus prolifreometer and the average grain size of target material grown on substrate, derived from AFM data is as tabulated in Table 2

The formation of spinel phase in thin film, which could not be judged entirely using the single peak XRD data owing to highly textured nature of the film, was confirmed by Raman spectroscopic technique. The Raman spectra of deposited thin film are shown in Fig. 3

Spinel ferrites in crystalline form arrange itself in a cubic structure that belongs to the space group O_h^7 (*Fd3m*). Although a full unit cell occupy 56 atoms ($Z=8$), the smallest Bravais cell in crystal lattice consists only of 14 atoms ($Z=2$). As a result, the factor group analysis predicts the following modes in a spinel structure [24]:

$$A1_g(R)+E_g(R)+F1g+3F_{2g}(R)+2A_{2u}+2E_u+4F_{1u}(IR)+2F_{2u}$$

The emission from five first-order Raman active modes ($A_{1g}+E_g+3F_{2g}$), were observed in Raman spectra of thin film sample. In cubic spinel ferrites, the modes at above 600 cm^{-1} is expected to match up with motion of oxygen in tetrahedral AO4 groups [25]. So the prominent mode at 607 cm^{-1} can be reasonably considered as A_{1g} symmetry. The other four low frequency modes represent the characteristics of octahedral sites (BO6). Therefore the observation of five Raman emission peaks originating from five first-order Raman active modes ($A_{1g}+E_g+3F_{2g}$) confirm formation of spinal phase in thin film.

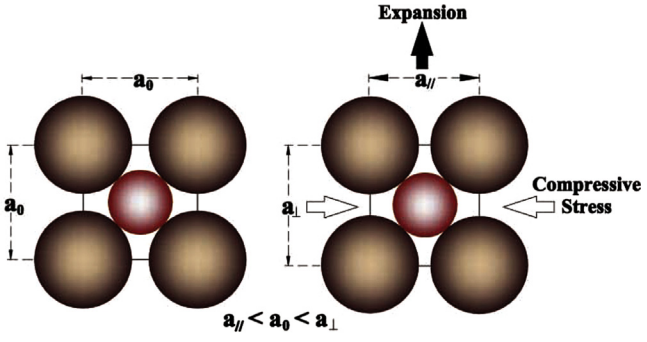

Fig. 2. Effect of the stress on the lattice parameter.

Table 2
Thickness and particle size of thin film.

Thickness (Å)	Particle size *D* (nm)
1422	47

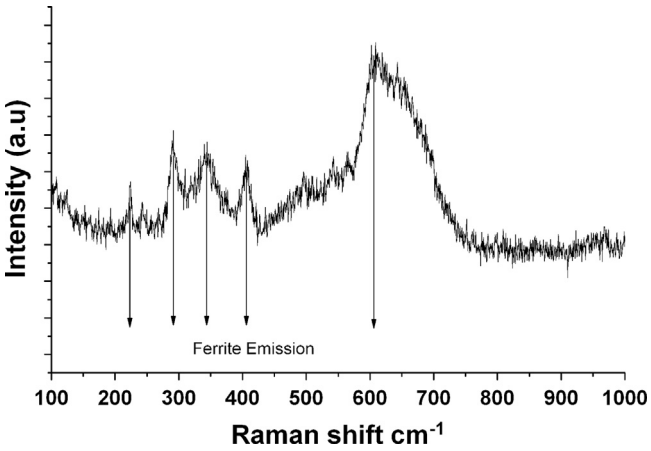

Fig. 3. Raman spectra of $Mn_{0.2}Zn_{0.8}Fe_2O_4$ thin film.

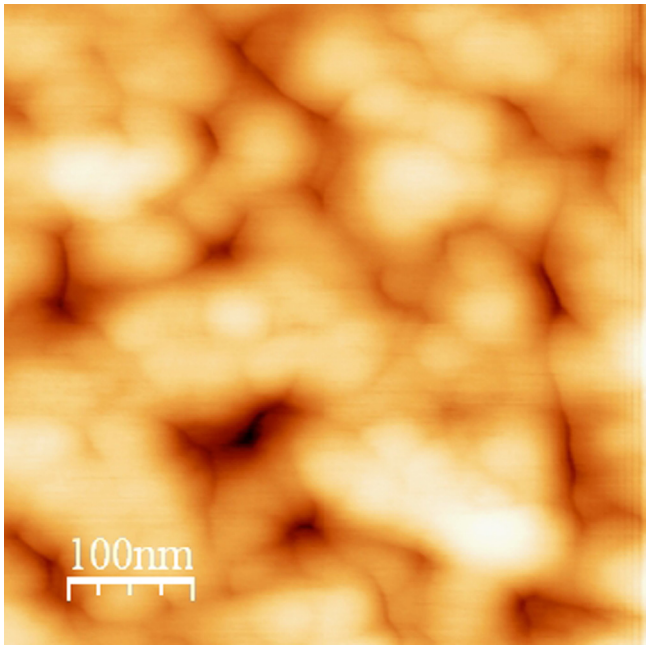

Fig. 4. AFM images of $Mn_{0.2}Zn_{0.8}Fe_2O_4$ thin film.

The particles size and surface morphology of the film were observed using AFM images (Figs. 4 and 5). AFM analysis of the thin film showed homogeneous morphology surface with spherical particles' of regular size and uniform distribution. The particles diameters on the thin film surface were measured at different points by a particle analysis tool and the average size calculated was 47 nm which is comparable to the size of the nanoparticles in the target material. The roughness histogram of the AFM image is as shown in Fig. 6. The high level of roughness is attributed to the formation of a ridge like morphology which is predominantly visible in the AFM image of the sample.

The reason for ridge like morphology observed in the AFM image is explained in a twin phenomenon approach. The target material which is highly stable is ablated using PLD, transported in the plume and deposited onto the substrate. The substrate being quartz an amorphous material, the expected nucleation sites for the growth of the film appear to be the first arrived target species which are deposited onto the substrate. The unit species on

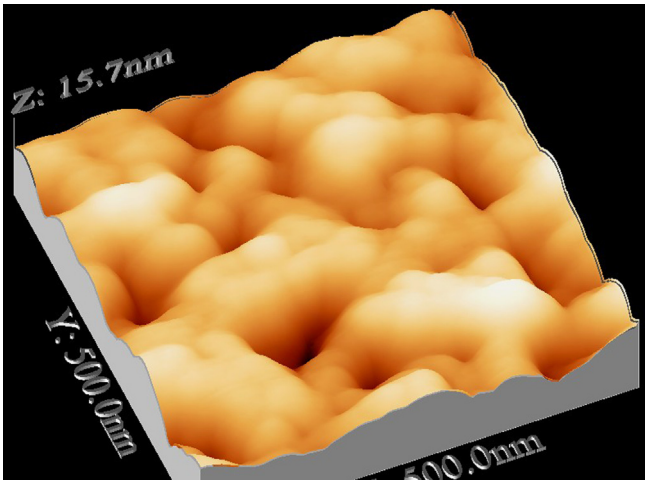

Fig. 5. 3D AFM image of $Mn_{0.2}Zn_{0.8}Fe_2O_4$ thin film.

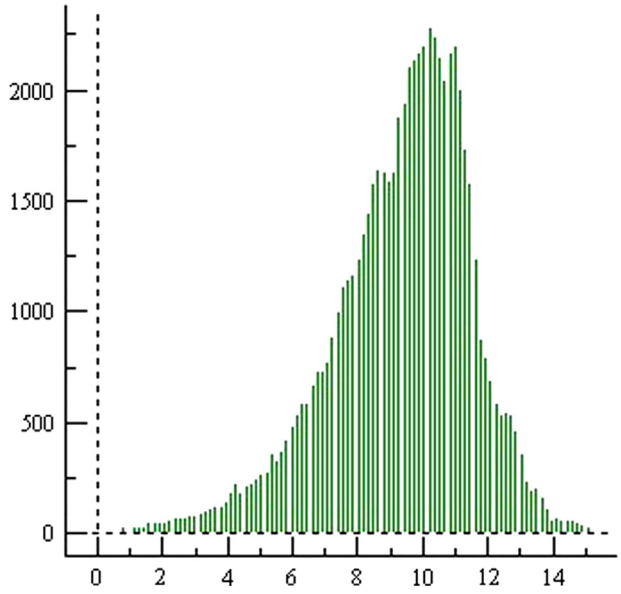

Fig. 6. Roughness histogram of $Mn_{0.2}Zn_{0.8}Fe_2O_4$ thin film. Horizontal scale:-.height (nm) and vertical scale:-number of events.

reaching the substrate plane lose their velocity component normal to the substrate and are physisorbed (weakly bound) onto the surface. The adsorbed species are not in equilibrium with each other and migrate on the surface (2-d gas) until they interact with other adsorbed species and form clusters. These clusters continue to grow until they reach a critical radius where they are thermodynamically stable which form the nuclei. The number of nucleation sites depends on adsorption properties of the target material, substrate, its combination and the physical parameters such as ambient pressure, substrate temperature, incoming species energy etc. Less nucleation sites provide an opportunity for directional growth which is optimized by a suitable selection of physical environmental parameters during growth which resulted in creation of the highly textured film.

A high deposition pressure and the use of Laser plume confined to a small area for transportation of the target species make it possible to obtain a certain level of porosity in deposited films. This can be explained by the fact that the flow of particles extracted from the target is concentrated onto a small volume (due to the confinement of particles in plume), which increases the number of particle collisions occurring in the space between the target and the substrate resulting in an increase of mean incident angle θ_2 (see Fig. 7). This can lead to the generation of shadowing effects leading to creation of intergranular voids within a growing layer. This along with the formation of ridge like morphology due to the directional growth described earlier contributes to the high level of roughnes on the surface of the film.

Magnetic properties of ferrite thin films depend on the magnetic-crystalline anisotropy, the grain size and surface morphology of the films. The *M–H* loop of the thin film recorded at room temperature with sample in-plane with magnetic field is shown in Fig. 8.

The substrate contribution to the *M–H* loop was subtracted after obtaining the loop. It can be seen that the material is magnetically ordered in the thin film format at room temperature and fully saturates at higher applied magnetic fields. The *X* and *Y*-axis intercept values indicative of coercivity and remnant magnetization of thin film sample with reasonably low hysteresis loss factor is tabulated in Table 3.

It is observed that our fabricated ferrite material in thin film format poses a relatively high value of coercivity in comparison to the reported value of 140 Oe [26]. A substantial shift in the XRD peak position for thin film sample indicating the presence of relatively large lattice strain, along with morphology disturbance noticed in AFM data explained in principle by taking into account the directional film growth and generation of shadowing effect leading to creation of intergranular voids, may be the major

Table 3
Coercivity and remnant magnetization of thin film sample.

X-axis intercept	*Y*-axis intercept
179.53	6.01×10^{-5}
−173.94	-5.82×10^{-5}

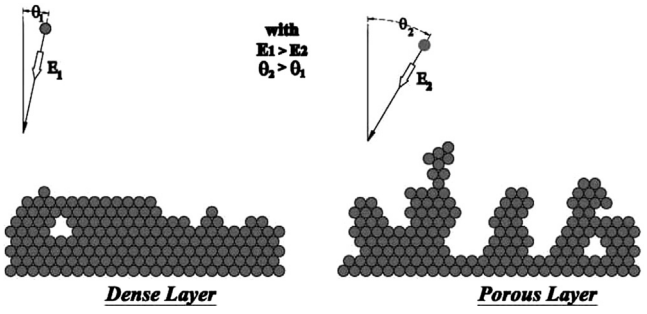

Fig. 7. Shadowing effect leading to creation of intergranular voids.

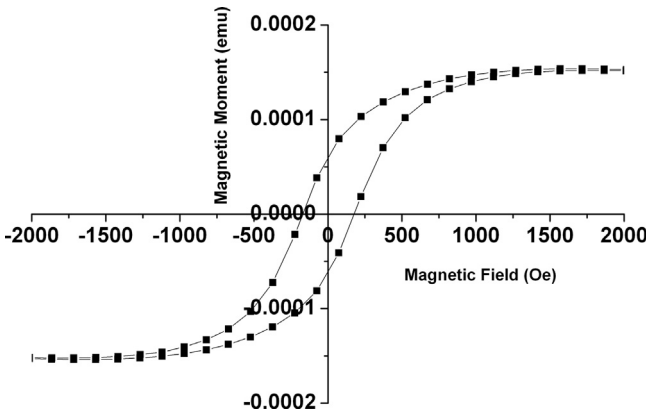

Fig. 8. *M–H* loops of $Mn_{0.2}Zn_{0.8}Fe_2O_4$ thin film.

contribution in creation of large magnetic anisotropy which eventually lead to the observation of high coercivity [21–23,26,27].

4. Conclusion

Highly textured $Mn_{0.2}Zn_{0.8}Fe_2O_4$ thin film was grown on quartz substrate using polycrystalline ferrite nanoparticle material as the target by PLD technique. The film was characterized using XRD and Raman spectroscopic techniques. The blue shift observed for 311 XRD peak, arising out of swing towards large inter-reticular distance, is explained with the help of atomic peening phenomena. Film particle size estimation from AFM data was corroborated with the size of nanoparticles in the target material. Morphology disturbance noticed in AFM data is caused by directional film growth and porosity generated from shadowing effects leading to creation of intergranular voids. The *M–H* loop of thin film recorded at room temperature revealed an enhancement in coercivity which is attributable to texture enhanced lattice strain and surface disorder originated from thin film growth mechanism. Thus, the present work can provide an effective approach to grow high quality ferrite thin films in processes compatible with integrated circuit technology on amorphous substrates wherein high value of coercivity find potential industrial applications.

Acknowledgments

The first author acknowledges the use of PLD, XRD, GIXRD, AFM, and SQUID VSM from UGC-DAE-CSR Indore.

References

[1] C.M. Williams, D.B. Chrisey, P. Lubit, J. Appl. Phys. 75 (1994) 1676.
[2] Y. Suzuki, et al., Appl. Phys. Lett. 68 (1996) 714.
[3] H. Mikami, Y. Nishikawa, Y. Omata, Proceedings of International Conference on Ferrites, Vol.7, 1996, p.126.
[4] P.J. van der Zaag, J.M.M. Ruigrok, M.F. Gillies, Philips J. Res. 51 (1998).
[5] T. Kiyomura, M. Gomi, Jpn. J. Appl. Phys. 36 (1997) 1000.
[6] R.G. Welch, J. Neamtu, M.S. Rogalski, S.B. Palmer, Mater. Lett. 29 (1996) 199.
[7] Y. Suzuki, R.B. van Dover, E.M. Gyorgy, Julia M. Phillips, V. Korenivski, Appl. Phys. Lett 68 (1996) 714.
[8] C.M. Williams, D.B. Chrisey, P. Lubitz, K.S. Grabowski, C.M. Cotell, J. Appl. Phys. 75 (1994) 1676.
[9] M. Koleva, R. Tomov, S. Zotova, P. Atanasov, C. Martin, C. Ristoscu, I. Mihailescu, Vacuum 58 (2000) 294.
[10] N. Yamazoe, Sens. Actuators B: Chem. 5 (1991) 7.
[11] W. Gopel, D. Schierbaum, Sens. Actuators B: Chem. 26 (1995) 203.
[12] G. Behr, W. Fhegel, Sens. Actuators B: Chem. 33–37 (1995) 2627.
[13] C.H. Kwon, H.-K. Hong, D.H. Yun, K. Lee, S.-T. Kim, Y.-H. Roh, B.-H. Lee, Sens. Actuators B: Chem. 24–25 (1995) 610.
[14] G. Magamma, V. Jayaraman, T. Gnanasekaran, G. Periaswami, Sens. Actuators B: Chem. 53 (1998) 133.
[15] S. Miyanishi, N. Iketani, K. Takayama, K. Innami, I. Suzuki, T. Kitazawa, Y. Ogimoto, Y. Murakami, IEEE Trans. Magn. 41 (2005) 2817.
[16] M.C. Williams, B.D. Chrisey, P. Lubits, S.K. Grabowski, M.J. Cotell, Appl. Phys. 75 (1994) 1676.
[17] P. Meakin, Fractals, Scaling, and Growth Far from Equilibrium, Cambridge University Press, Cambridge, 1998.
[18] M. Kardar, G. Parisi, Y.C. Zhang, Phys. Rev. Lett. 56 (1986) 889.
[19] D.J. Srolovitz, Acta. Mater. 37 (1989) 621;
G. Palasantzas, J. Th. M. De Hosson, Appl. Phys. Lett. 78 (2001) 3044.
[20] T. Scharf, J. Faupel, K. Sturm, H.U. Krebs, J. Appl. Phys. 94 (2003) 4273.
[21] A. Lisfi, C.M. Williams, J. Appl. Phys. 93 (2003) 8143.
[22] A. Lisfi, J.C. Lodder, E.G. Keim, C.M. Williams, Appl. Phys. Lett. 82 (2003) 76.
[23] H. Waqas, X.L. Huang, J. Ding, H.M. Fan, Y.W. Ma, T.S. Hemg, A.H. Quresh, J.Q. Wei, D.S. Xue, J.B. Yi, J. Appl.Phys. 107 (2010) 09A514-1.
[24] Zhongwu Wang, David Schiferl, Yusheng Zhao, H.St.C. O'Neill, J. Phys. Chem. Solids 64 (2003) 2517–2523.
[25] Z.W. Wang, P. Lazor, S.K. Saxena, G. Artioli, J. Solid State Chem. 165 (2002) 165–170.
[26] Y.P. Zhao, R.M. Gamache, G.-C. Wang, T.-M. Lu, G. Palasantzas, J.Th.M. De Hosson, J. Appl. Phys. 89 (2001) 1325.
[27] Y.P. Zhao, G. Palasantzas, G.C. Wang, T.M. Lu, J. Th, M. De Hosson, Phys. Rev. B 60 (1999) 1216.